



## Article

# Comprehensive Analyses of PPP-B2b Performance in China and Surrounding Areas

Yan Liu, Cheng Yang \* and Mengni Zhang

School of Land Science and Geomatics, China University of Geosciences, Beijing 100083, China; 2012190026@cugb.edu.cn (Y.L.); 2112210060@email.cugb.edu.cn (M.Z.)

\* Correspondence: c.yang@connect.polyu.hk

**Abstract:** BeiDou Global Navigation Satellite System (BDS-3) provides a regional Precise Point Positioning (PPP) service, called PPP-B2b, for users in China and surrounding areas through B2b signal transmitted from its three geostationary earth orbit (GEO) satellites. The information broadcasted by the B2b signal include satellite orbit corrections, satellite clock offset corrections, and differential code bias (DCB) corrections of BDS-3 satellites. In this study, the accuracies of PPP-B2b corrections along with real-time PPP performance are comprehensively evaluated referenced to precise orbit and clock products from GFZ and the precise DCB products from CAS. The result indicates that the accuracy of the BDS-3 broadcast orbit is similar to that of the PPP-B2b real-time orbit. The PPP-B2b clock offset correction improved the satellite clock offset precision of the BDS-3 broadcast ephemeris. The Signal-in-Space Range Error (SISRE) of broadcast ephemeris and PPP-B2b are calculated, which are 0.536 and 1.24 m, respectively. The large SISRE value of PPP-B2b is caused by the satellite-specified systematic bias to IGS final products. The positioning performance evaluation of real-time PPP with B2b service is carried out and compared with the real-time product provided by Wuhan University (WHU) based on the eight IGS MGEX stations in China and surrounding countries. The positioning accuracy of static positioning mode with PPP-B2b service achieved centimeter-level accuracy in the selected station, and that of kinematic positioning mode achieved decimeter-level accuracy. The availability rate of PPP-B2b corrections in the surrounding area of China, however, degrades from 88.76% to 60.91% in the selected stations. The accuracy of the PPP solution using PPP-B2b correction is better than that of using WHU real-time product within China. The positioning performance of stations located at the boundary of the PPP-B2b service area, however, is affected by the number of PPP-B2b available satellites. The positioning accuracy in kinematic positioning mode is worse than that of using WHU real-time precise product.

**Keywords:** BDS-3; PPP-B2b; real-time PPP; matching strategy; accuracy assessment



**Citation:** Liu, Y.; Yang, C.; Zhang, M. Comprehensive Analyses of PPP-B2b Performance in China and Surrounding Areas. *Remote Sens.* **2022**, *14*, 643. <https://doi.org/10.3390/rs14030643>

Academic Editors: Yunbin Yuan and Baocheng Zhang

Received: 8 December 2021

Accepted: 26 January 2022

Published: 28 January 2022

**Publisher's Note:** MDPI stays neutral with regard to jurisdictional claims in published maps and institutional affiliations.



**Copyright:** © 2022 by the authors. Licensee MDPI, Basel, Switzerland. This article is an open access article distributed under the terms and conditions of the Creative Commons Attribution (CC BY) license (<https://creativecommons.org/licenses/by/4.0/>).

## 1. Introduction

BeiDou Navigation Satellite System (BDS), like other Global Navigation Satellite Systems (GNSSs), aims to provide positioning, navigation, and timing (PNT) services for global users [1]. The initial BDS demonstration navigation system (BDS-1) was established in 2003, and it consisted of three geostationary orbit (GEO) satellites. The system provided positioning, timing, and short message communication services with transparency retransmission mode. The BDS regional navigation satellite system (BDS-2) started its service on 27 December 2012. The constellation consisted of five GEO satellites, five inclined geosynchronous orbit (IGSO) satellites, and four medium Earth orbit (MEO) satellites. BDS-2 broadcasted three frequency signals, 1561.098 MHz (B1I), 1207.140 MHz (B2I), and 1268.520 MHz (B3I), covering the Asia-Pacific region. The BDS-2 continued the services of BDS-1, and further provided kinematic positioning in three dimensions. The global constellation of BDS-3 completed on 23 June and provided global service on 31 July 2020. The constellation consists of 24 MEO satellites, 3 GEO satellites, and 3 IGSO satellites. The

system not only broadcasts the B1I and B3I signals, but also broadcasts 1575.420 MHz (B1C), 1207.140 MHz (B2b), and 1176.45 MHz (B2a) by MEO satellites for global positioning users [2]. In addition to providing global PNT services, regional and global short message communications (SMC) services, the international search and rescue (SAR) services, and regional precise point positioning (PPP) services are also provided. The service coverage area of PPP-B2b is between 80° E and 155° E longitude, 5° S and 55° N latitude [3]. The correction parameters contain precise orbit correction parameters, clock offset correction parameters, and differential code bias (DCB).

PPP is able to achieve decimeter or centimeter-level positioning accuracy using a standalone GNSS receiver with precise satellites orbit and clock products [4–9]. Currently, the real-time services (RTS) of International GNSS services (IGS) provides the precise satellite orbit and clock products to global users through the internet. The internet connection, however, affects the integrity of the correction data, which further affects the performance of PPP. In addition to IGS RTS, commercial companies, such as StarFire of NavCom and RTX of Trimble, also provide RTS for PPP by broadcasting the correction parameters via satellites communication links [10–13]. The cost requirement of satellite-based RTS limited the application to ordinary users. Furthermore, the Galileo satellite system can also provide decimeter horizontal positioning accuracy by shortening the ephemeris updating rate, resulting in smaller SISRE [14]. The BDS-3, however, provides a regional PPP service in a different way (called PPP-B2b) using the accurate ephemeris broadcast by B2b signals of GEO satellites, which allows users to perform PPP for free and without the internet.

The performances of the PPP-B2b service have been evaluated with the stations within China territory. A software-defined receiver is used to evaluate the performance of the BDS-3 real-time PPP service. It is stated that the PPP-B2b signal can provide a stable PPP service for users in the Asia-Pacific region with decimeter to centimeter-level orbit corrections and meter-level clock corrections [15]. Referenced to precise ephemeris products from Deutsches GeoForschungsZentrum (GFZ), Germany and RTS of Centre National d'Etudes Spatiales (CNES), France, some performance evaluation studies on the PPP-B2b proved that the PPP-B2b can achieve decimeter or centimeter-level accuracy for static and kinematic positioning [16–18]. A comprehensive evaluation for PPP-B2b performance, in terms of message matching strategy, service availability, and correction accuracy, has been conducted [10]. The study further analyzes the decimeter and centimeter-level positioning accuracy of PPP-B2b with different ionosphere-free (IF) combinations. Usually, most performance evaluations of the PPP-B2b have been focused on the selected IGS or international GNSS Monitoring and Assessment System (iGMAS) stations within China territory. The real-time performance of the BDS-3 PPP-B2b service around China, however, needs to be further evaluated. In this paper, the BDS-3 real-time PPP-B2b performance, in terms of availability and accuracy, is assessed by the stations located in China and the surrounding countries, such as Korea, Japan, and Mongolia. The performance of PPP-B2b is also compared with solutions acquired from the real-time product of Wuhan university (WHU).

The paper is organized as follows: in Section 2, the PPP-B2b correction parameters and the corresponding matching strategy are briefly described. The performance assessment methods for PPP-B2b correction parameters are described in detail. In addition, the IF model of real-time PPP is also introduced to evaluate the positioning performance of the real-time PPP service of BDS-3. In Section 3, the accuracy of the PPP-B2b satellite orbit correction, and clock offset correction are evaluated and compared to the real-time product from WHU. The SISRE and orbit only SISRE of broadcast ephemeris, PPP-B2b correction product are then calculated and compared to that of real-time product from WHU, and the DCB corrections are evaluated as well. The positioning performance assessment and comparison to WHU real-time products are performed. Finally, some conclusions are summarized.

## 2. Methodology

In this section, the correction message of PPP-B2b is briefly introduced, and the matching strategies of the correction parameter are presented. The correction models of the satellite orbit, satellite clock, and code bias are discussed afterward. Finally, the performance assessment methods of PPP-B2b are presented, in terms of orbit accuracy, clock offsets, SISRE, and differential code bias, as well as the PPP IF model.

### 2.1. PPP-B2b Correction Message and Matching Strategy

The PPP-B2b signals of the GEO satellites of BDS-3 broadcast five parameters: satellite mask, satellite orbit and clock offset corrections, DCB, and user range accuracy index (URAI). These five parameters and corresponding message types, along with nominal validities, which indicate the validate durations of information, are listed in Table 1 [19]. The update rate of satellite orbit and clock offset corrections are 48 and 6 s, respectively [19].

Table 1. PPP-B2b message information.

Information Content	Message Type	Nominal Validity(s)
Satellite mask	1	–
Orbit correction	2,6,7	96
DCB	3	86,400
Clock correction	4,6,7	12
URAI	2,5,6,7	96

To ensure the correct matching between the correction information and the broadcast ephemeris, the Issue of Data (IOD) is employed as a matching indicator. These IODs include: IOD of state space representation (IOD SSR), IOD of pseudo-random noise mask (IODP), and IOD of navigation (IODN), as well as the IOD of orbit and clock corrections (IOD Corr). The matching strategy is illustrated in Figure 1. It should be noted that the DCB parameter is not included in this matching strategy because it does not change within a day.

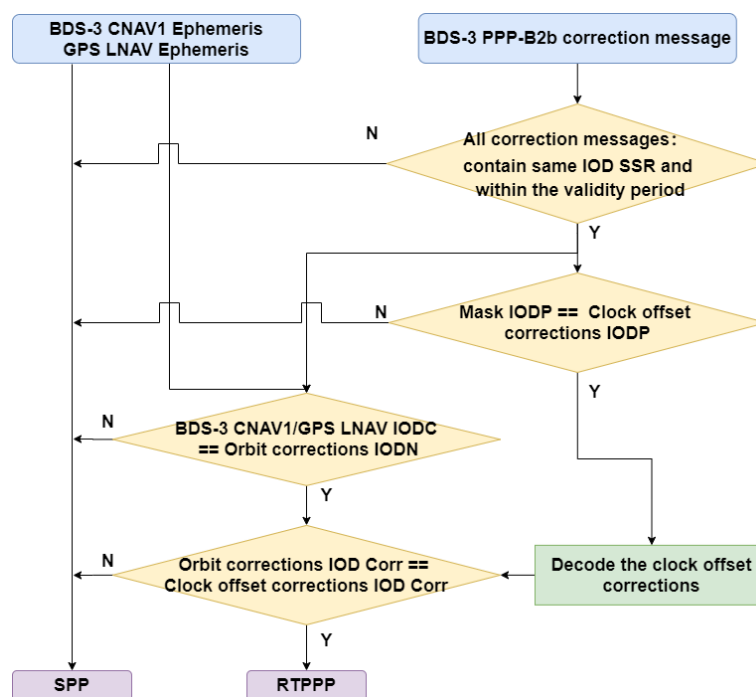


Figure 1. Matching strategy.

As shown in Figure 1, the retrieved IOD SSRs from those messages should remain consistent with each other, and the received PPP-B2b correction messages should be within the nominal validity period as listed in Table 1. To acquire the correct satellite clock correction information, the satellite PRN is decoded if the same IODP is acquired from message types 1 and 4. The satellite clock correction index and IOD Corr of the certain satellite could be obtained from message type 4 afterward. The orbit correction information, including satellite PRN, corresponding IOD Corr, and related IODN, can be acquired from message type 2. If the IODN matches the IOD of clock (IODC) from the broadcast ephemeris, and the IOD Corr from orbit correct information matches that from clock correction information, the precise orbit and clock correction can be used for the real-time PPP solution.

## 2.2. PPP-B2b Correction Message Evaluation Methods

The satellite orbit correction message of the PPP-B2b contains the orbit correction vector  $\delta O = [\delta O_r, \delta O_a, \delta O_c]^T$  in radial, along-track, and cross-track components, respectively. The real-time precise orbit thus can be obtained by transforming the correction vector to the Earth-Center-Earth-Fixed (ECEF) frame as expressed in Equations (1) and (2) [19],

$$\delta X = \begin{bmatrix} e_{radial} & e_{along} & e_{cross} \end{bmatrix} \delta O$$

$$e_{radial} = \frac{r^s}{|r^s|} \quad (1)$$

$$e_{cross} = \frac{r^s \times v^s}{|r^s \times v^s|}$$

$$e_{along} = e_{cross} \times e_{radial}$$

$$X_{pre,B2b} = X_{brdc} - \delta X \quad (2)$$

where  $\delta X$  is the orbit correction vector in ECEF coordinate system;  $r^s$  and  $v^s$  are the satellite position and velocity vectors calculated from the broadcast ephemeris, respectively;  $X_{brdc}$  is the satellite position vector from the broadcast ephemeris in the ECEF frame;  $X_{pre,B2b}$  is the corrected real-time precise satellite position vector in the ECEF frame.

The clock offset correction is directly related to the satellite clock offset obtained from the broadcast ephemeris. Hence, the real-time precise satellite clock offset can be retrieved directly [19],

$$dt_{pre,B2b}^s = dt_{brdc}^s - \frac{C_0}{c} \quad (3)$$

where  $dt_{pre,B2b}^s$  is the precise satellite clock offset corrected by PPP-B2b correction message;  $dt_{brdc}^s$  is the satellite clock offset derived from the broadcast ephemeris;  $C_0$  is the PPP-B2b clock correction value;  $c$  is the velocity of light.

DCB is caused by code-based hardware delay difference between different frequencies, and affects the performance of PPP [20]. The DCB could be corrected by broadcast PPP-B2b correction messages [19],

$$\tilde{P}_{freq} = P_{freq} - DCB_{freq} \quad (4)$$

where  $\tilde{P}_{freq}$  is the corrected pseudorange observation of the certain frequency  $freq$ ;  $P_{freq}$  is the observed pseudorange value;  $DCB_{freq}$  is the PPP-B2b DCB corrections for corresponding signals of BDS-3 in meters.

To evaluate the performance of satellite orbit, clock offset and DCB recovered from the PPP-B2b messages, the final products from GFZ and the Chinese Academy of Sciences (CAS) are used as a reference. IGS also initiated the experimental multi-GNSS orbit combination service [21], however, only precise orbit products are available at the present stage. Thus, in the study, the precise orbit and clock product from GFZ are employed as reference. The accuracy of BDS-3 broadcast ephemeris, and PPP-B2b real-time orbit and clock offset, are further compared to WHU real-time products. The precise orbit product from GFZ is referred to the center-of-mass (CoM) of the satellite, while the BDS-3 precise orbit

information retrieved from the PPP-B2b message referred to the antenna phase center (APC) of the satellite [22]. Therefore, the phase center offset (PCO) correction between the GFZ final orbit and the PPP-B2b orbit should be employed. The precise orbit error of the PPP-B2b with respect to GFZ final product can be written as [23],

$$\delta X_{pre} = X_{pre,GFZ} - [X_{pre,B2b} + A \cdot \delta X_{pco}] \quad (5)$$

where  $\delta X_{pre}$  is the precise orbit error vector;  $X_{pre,GFZ}$  is the reference orbit vector obtained from GFZ;  $X_{pre,B2b}$  is the real-time PPP-B2b precise orbit vector;  $A$  is the satellite attitude matrix;  $\delta X_{pco}$  is the satellite PCO correction vector obtained from the latest "igs14.atx" file released by IGS. The orbit error vector in satellite radial, along-track, and cross-track components then can be expressed as,

$$\delta O_{pre} = [e_{radial} \ e_{along} \ e_{cross}]^T \cdot \delta X_{pre} \quad (6)$$

where  $\delta O_{pre}$  is the satellite precise orbit error vector in radial, along-track, and cross-track components with respect to the final product from GFZ; other parameters are defined as above.

The PPP-B2b satellite clock offset is compared to precise clock offset products from GFZ. The timescale and frequency references of the GFZ final satellite clock offset products, however, are different from those of the PPP-B2b satellite clock offset. The GPS system time (GPST) is adopted for the GFZ final clock product rather than the BDS time (BDT). The time offset, 14s, between the different time systems needs to be compensated before the evaluation. Moreover, the final satellite clock offset of GFZ uses the B1I and B3I IF combination as the reference signal, while the PPP-B2b satellite clock offset is referred to B3I signal frequency [18,24]. Hence, the corrections of the satellite hardware delays should be applied, which referred to the broadcasted DCB from PPP-B2b signals [25],

$$\delta t_{pre,B2b}^s = dt_{pre,B2b}^s - \frac{f_{B1I}^2}{f_{B1I}^2 - f_{B3I}^2} DCB_{B1I}^s \quad (7)$$

where  $\delta t_{pre,B2b}^s$  is the PPP-B2b satellite clock offset referred to B1I/B3I IF combination after DCB correction;  $f_{B1I}^2$  and  $f_{B3I}^2$  are the frequencies of B1I and B3I signals, respectively.

The difference in the satellite clock offsets between the PPP-B2b ephemeris and the GFZ products is

$$\Delta \delta t^s = \delta t_{pre,B2b}^s - \delta t_{pre,GFZ}^s \quad (8)$$

where the  $\Delta \delta t^s$  is the satellite clock offset difference between PPP-B2b ephemeris and GFZ final clock product of the satellite  $s$ ; the  $\delta t_{pre,GFZ}^s$  is the precise satellite clock offset calculated by GFZ final products.

The precise satellite clock offset products from different analysis centers (ACs), however, have timescale differences. This systematic error is commonly reduced by subtracting the clock offset of the reference satellite [26]. In our case, it is hard to evaluate the PPP-B2b satellite clock offset based on a fixed reference satellite with 24 h continuous availability. Thus, the clock systematic error is reduced by subtracting the average clock offset from  $\Delta \delta t^s$  at each epoch, which forms the single difference between the PPP-B2b clock offset and the precise clock offset from GFZ,

$$\nabla \Delta \delta t^s = \Delta \delta t^s - \frac{1}{M} \sum_{i=0}^M \Delta \delta t^i \quad (9)$$

where  $\nabla \Delta \delta t^s$  is the clock offset difference sequence;  $M$  is the available satellite number from PPP-B2b signal at each epoch. However, the available satellite number  $M$  may change at each epoch. The time sequence of  $\nabla \Delta \delta t^s$  becomes discontinuous which affects the

reliability of clock offset standard deviation (STD). Therefore, the time series  $\nabla\Delta\delta_t^s$  needs to be re-edited properly [17],

$$\begin{aligned} \widetilde{\nabla\Delta\delta_t^s} &= \nabla\Delta\delta_t^s - \Delta D_{t,t-1} \\ \Delta D_{t,t-1} &= \begin{cases} \frac{1}{M} \sum_{i=0}^M \Delta\nabla\Delta\delta_{t,t-1}^i & \left| \frac{1}{M} \sum_{i=0}^M \Delta\nabla\Delta\delta_{t,t-1}^i \right| \geq 0.1ns \\ 0 & \left| \frac{1}{M} \sum_{i=0}^M \Delta\nabla\Delta\delta_{t,t-1}^i \right| < 0.1ns \end{cases} \quad (10) \\ \Delta\nabla\Delta\delta_{t,t-1}^i &= \nabla\Delta\delta_t^i - \nabla\Delta\delta_{t-1}^i \end{aligned}$$

where  $\widetilde{\nabla\Delta\delta_t^s}$  is the re-edited time sequence;  $\Delta D_{t,t-1}$  is the systematic error compensation term which is significantly affected by the number of available satellites;  $\Delta\nabla\Delta\delta_{t,t-1}^i$  is the time difference of  $\nabla\Delta\delta_t^i$  between epochs  $t$  and  $t - 1$  for satellite  $i$ .

The signal-in-space range error (SISRE) is a key performance indicator for PPP-b2b orbit and clock errors [25]. Usually, the global average SISRE is employed to evaluate the performances of different constellations and different precise products [14,27–31]. In this study, the SISRE of broadcast ephemeris, PPP-B2b corrected orbit, and clock and WHU real-time product are calculated based on the following equation [31],

$$SISRE = \sqrt{(RMS(w_R\delta_R - \delta_T))^2 + w_{A,C}^2(A^2 + C^2)} \quad (11)$$

where  $w_R$  and  $w_{A,C}^2$  are constellation-specific weight factors with values of 0.98 and 1/54 for BDS-3 [17,22];  $\delta_R$  is the radial error components;  $\delta_T$  is the satellite clock error with respect to GFZ final clock product;  $A, C$  are the RMS of along-track and cross-track error components, respectively. The orbit-only SISRE for BDS-3 MEO satellites are also calculated to evaluate the performances of PPP-B2b real-time orbits

$$SISRE_{orbit} = \sqrt{w_R^2\delta_R^2 + w_{A,C}^2(A^2 + C^2)} \quad (12)$$

The DCB corrections broadcasted by PPP-B2b can be evaluated by comparing with precise MGEX DCB products derived by the Chinese Academy of Sciences (CAS). The CAS DCB products currently provide DCB corrections for BDS-3 satellites from C19 to C46 with approximately 0.17 ns stability over a month [32]. The relationship between the PPP-B2b DCB corrections and the CAS DCB corrections can be expressed by the following expression [33],

$$\begin{aligned} DCB_{B1I,B2b} &= DCB_{C2I-C6I,CAS} \\ DCB_{B1Cp,B2b} &= DCB_{C1P-C6I,CAS} \\ DCB_{B2ap,B2b} &= DCB_{C1P-C6I,CAS} - DCB_{C1P-C5P,CAS} \end{aligned} \quad (13)$$

where  $DCB_{sig,B2b}$  and  $DCB_{sig1-sig2,CAS}$  are the DCB corrections obtained from PPP-B2b service and CAS final products, respectively. The subscripts C2I and C6I denote B1I and B3I signals, respectively; C1P denotes B1Cp signal; C5P denotes B2ap signal.

### 2.3. Real-Time IF-PPP Model with PPP-B2b Corrections

The performance of PPP-B2b signal is further evaluated with PPP positioning accuracy. The multi-frequency pseudorange and carrier phase observations at the  $i$ th frequency can be written as [34],

$$\begin{aligned} P_i &= \rho + c(dt_r - dt^s) + \frac{f_1^2}{f_i^2} I_1 + M_w \cdot T_{zwd} + T_{zhd} + B_{r,i} - B_i^s + \varepsilon_{P_i} \\ L_i &= \rho + c(dt_r - dt^s) - \frac{f_1^2}{f_i^2} I_1 + M_w \cdot T_{zwd} + T_{zhd} + \lambda_i(N_i + b_{r,i} - b_i^s) + \varepsilon_{L_i} \end{aligned} \quad (14)$$

where  $P_i$  and  $L_i$  are the observations of pseudorange and carrier phase at frequency  $f_i$ ;  $\rho$  is the geometric distance between satellite and receiver;  $c$  is the speed of light;  $dt_r$  and  $dt^s$  are the satellite and receiver clock offset, respectively;  $I_1$  is the ionospheric delay of  $L_1$ ;  $T_{zwd}$  is the zenith wet tropospheric delay and  $M_w$  is the corresponding mapping function;  $T_{zhd}$  is the zenith hydrostatic tropospheric delay;  $B_{r,i}$  and  $B_i^s$  are the pseudorange hardware delays of the receiver and satellite;  $\lambda_i$  and  $N_i$  are the wavelength and the integer ambiguity of frequency  $f_i$ ;  $b_{r,i}$  and  $b_i^s$  are the carrier phase hardware delays of the receiver and satellite;  $\varepsilon_{P_i}$  and  $\varepsilon_{L_i}$  are the observation noise and unmodeled errors of the pseudorange and carrier phase.

The receiver hardware delay can be absorbed in the receiver clock offset. The satellite clock offset and the satellite hardware delay can be compensated by PPP-B2b clock offset correction and DCB correction, respectively. The other errors, such as zenith hydrostatic tropospheric delay, relativistic effect, phase windup effect, Sagnac effect, are corrected by the corresponding model. Ignoring the observation noise, we write the linearized observation equation of the dual-frequency IF combination as [35],

$$\begin{aligned} P_{IFij} &= -e \cdot r + c \cdot \delta t_r + M_w \cdot T_{zwd} \\ L_{IFij} &= -e \cdot r + c \cdot \delta t_r + M_w \cdot T_{zwd} + \lambda_{IFij} N_{IFij} \end{aligned} \quad (15)$$

where  $P_{IFij}$  and  $L_{IFij}$  are the pseudorange and carrier phase IF combination values at  $f_i$  and  $f_j$  frequencies after error correction;  $e$  is the unit vector of receiver-to-satellite direction;  $r$  is the receiver position incremental vector;  $\delta t_r$  is the receiver clock offset contains receiver hardware delay;  $\lambda_{IFij}$  and  $N_{IFij}$  are the combined wavelength and the combined ambiguity which absorbs the carrier phase hardware delay and no longer has an integer characteristic. The error equation is then expressed as:

$$V = HX - l \quad (16)$$

where  $H$  is the design matrix;  $X = [ r \quad c \cdot \delta t_r \quad T_{zwd} \quad N_{IF} ]$  is the estimated parameters; and  $l$  is the measurements vector after the corresponding error has been modeled properly.

### 3. Experimental Evaluation

In this section, the MEO satellites of BDS-3 are used to evaluate the PPP-B2b performance, in terms of satellite orbit and clock, SISRE, as well as DCB accuracy, referenced to precise products from GFZ. The accuracy of the orbit and the clock offset of the GFZ precise products achieved centimeter-level accuracy for BDS-3 MEO satellites [36,37]. The accuracy of PPP-B2b real-time orbit and clock offsets are further compared to the real-time products from WHU. In addition to the accuracy assessment of the PPP-B2b correction message, the performance evaluation of the real-time PPP was also conducted with eight IGS stations distributed in the service area. The corresponding CNAV1 broadcast ephemerides of BDS-3 are downloaded from the Test and Assessment Research Center of China Satellite Navigation Office ([csno-tarc.cn/datacenter/ephemeris](http://csno-tarc.cn/datacenter/ephemeris), accessed on 7 December 2021).

#### 3.1. PPP-B2b Orbit Accuracy Assessment

The PPP-B2b orbit correction sequences of the MEO satellites of BDS-3 decoded from the PPP-B2b message on 9 August 2021 (DoY 221) are shown in Figure 2. The variations in orbit correction sequence for MEO satellites are within 0.1, 0.3, and 0.3 m in radial, along-track, and cross-track components, respectively. The centimeter-level corrections indicate that considerable accuracy could be achieved by the broadcast orbits of BDS-3 MEO satellites, which mainly benefits from the application of inter-satellite links (ISL) technology [38]. Figure 2 also reveals the hourly discontinuity of the orbit correction series, which is related to the hourly update of the broadcast ephemeris [39].

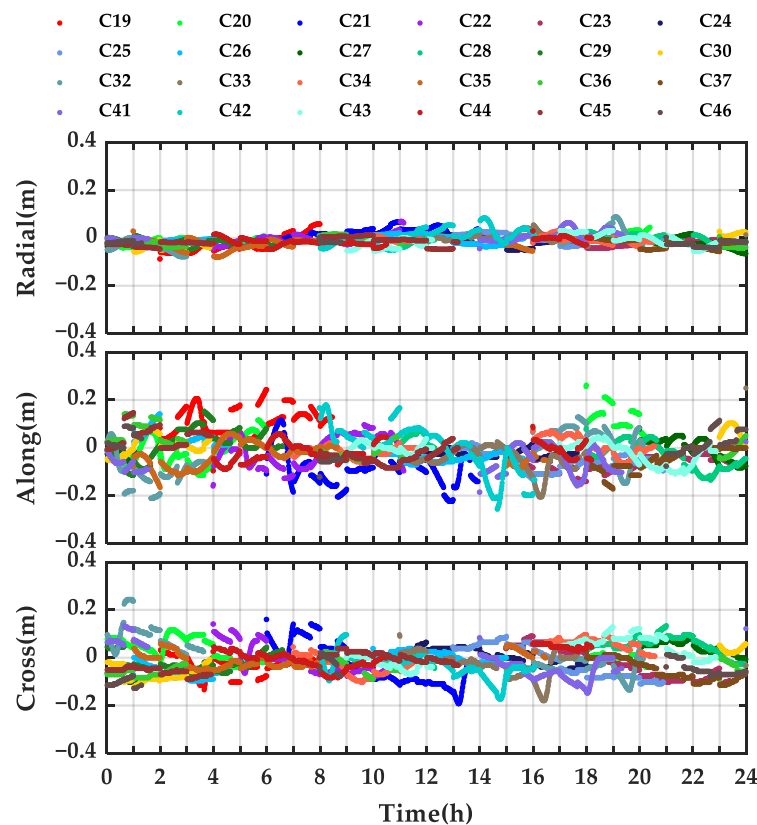


**Figure 2.** PPP-B2b orbit corrections of BDS-3 MEO on Doy 221.

The real-time orbit errors in radial, along-track, and cross-track components for the PPP-B2b referenced to the final precise orbit from GFZ are presented in Figure 3a, and those of broadcast ephemeris are presented in Figure 3b. The WHU real-time orbit errors referenced to GFZ final products are plotted in Figure 3c. The orbit errors for both real-time PPP-B2b orbit and broadcast orbit exhibit the same level of accuracy. The real-time orbit error series of PPP-B2b is smoother and more continuous than that of the broadcast orbit error. The orbit error of WHU real-time product is more continuous and smoother, and more consistent with the GFZ final orbit product. The satellite orbit errors of C41 and C42 of the PPP-B2b real-time orbits show some abnormal errors with 0.6 m in radial components, compared to the final precise orbit from GFZ. The significant difference in the orbits between the PPP-B2b and that of GFZ may relate to the PCO corrections released by IGS. To further analyze this orbit bias, the orbit errors in radial, along-track, and cross-track components that apply the PCO corrections provided by China Satellite Navigation Office (CSNO) are presented in Figure 4. The abnormal orbit error of the satellites C41 and C42 no longer exist, but satellite orbit C44 appeared to have a significant bias, with about 1 m, on the radial component. Thus, the significant biases on satellite orbits are related to difference in the PCO corrections, which do not participate in real-time PPP solutions with PPP-B2b signals.

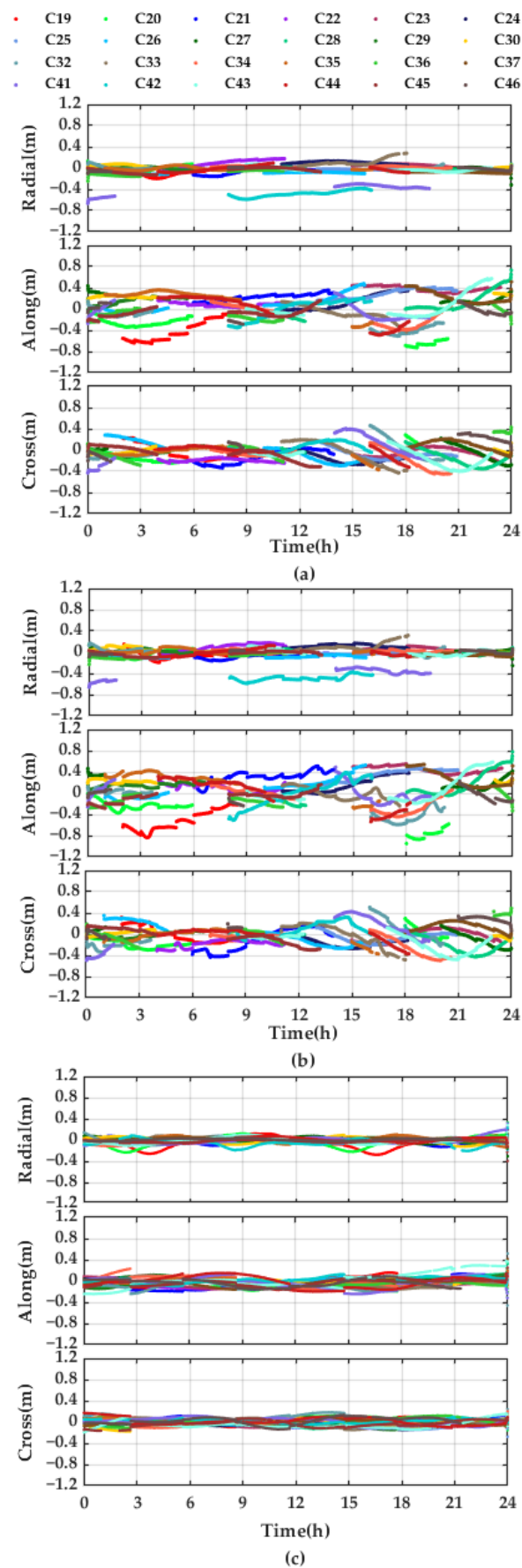
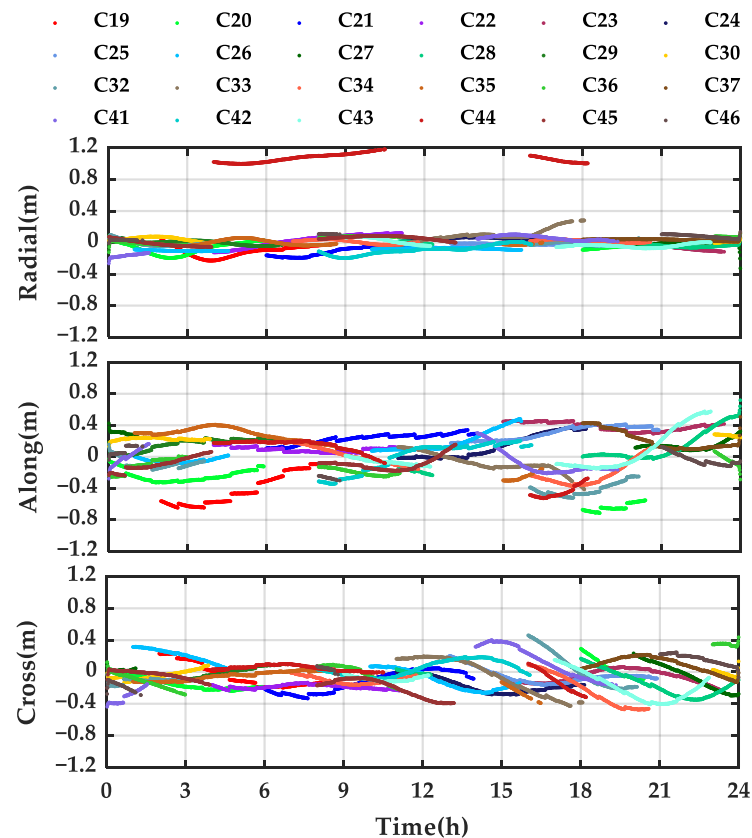


Figure 3. Orbit errors of PPP-B2b real-time orbit (a), broadcast orbit (b), and WHU real-time orbit (c).



**Figure 4.** Orbit errors of PPP-B2b orbit by applying PCO corrections from CSNO.

To further evaluate the accuracy of satellite orbits of PPP-B2b products, the Root Mean Square Error (RMSE) of PPP-B2b real-time orbits, broadcast orbits, and real-time orbits from WHU based on a 7-day dataset (6–12 August 2020) are presented in Figure 5. The RMSE of different satellite orbits also indicates that the radial components of both PPP-B2b orbit and broadcast orbit have better performance than that of the along-track and cross-track components. The higher accuracy on the radial component is mainly related to the high-quality onboard hydrogen and rubidium clocks, which compensate for the systematic error in the radial component [31]. The corresponding average RMSEs of the BDS-3 MEO satellites are listed in Table 2. The average RMSE of PPP-B2b orbits is 8.5, 19.3, 14.0 cm in radial, along-track, and cross-track components, respectively. The difference between the PPP-B2b orbit and the broadcast orbit is only centimeter-level. This slight accuracy improvement may be related to the better continuity of the PPP-B2b orbit than that of the broadcast orbit. The WHU real-time orbits exhibit better accuracy than that of PPP-B2b orbits. The RMSE of WHU real-time orbits on radial, along-track, and cross-track components are 4.6, 8.1, and 6.1 cm, respectively. The better accuracy of the WHU real-time orbit is mainly benefited by the global GNSS network, while the PPP-B2b service only relies on the regional monitoring stations in China.

**Table 2.** Mean orbit RMSEs (cm) of BDS-3 MEO.

RMSE	Radial	Along-Track	Cross-Track
PPP-B2b	8.5	19.3	14.0
Broadcast	8.8	20.7	15.4
WHU	4.6	8.1	6.1

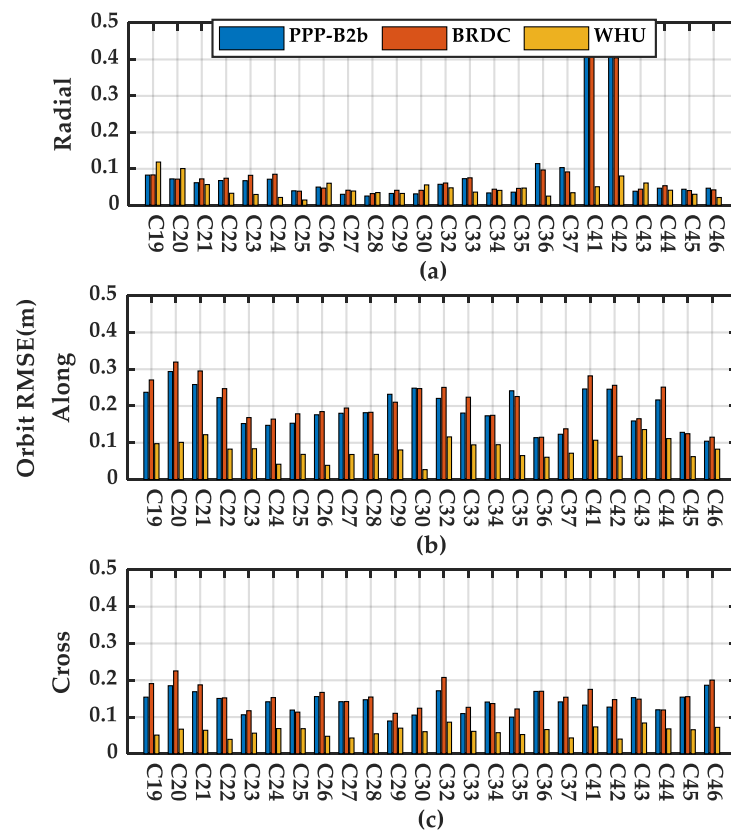


Figure 5. Orbit RMSEs of PPP-B2b orbit (a), broadcast orbit (b), and WHU real-time orbit (c).

### 3.2. PPP-B2b Clock Offset Accuracy Assessment

The PPP-B2b clock offset correction sequences of BDS-3 MEO satellites on DoY 221 are shown in Figure 6a. The PPP-B2b clock offset corrections of each satellite are within 3 m and contain systematic offsets. The details of clock offset correction parameters of satellites C24, C35, and C44 are presented in Figure 6b. It is easy to find that the corrections of these three satellites fluctuate around constant values of about  $-1$ ,  $2$ , and  $0$  m, respectively. The corrections also exhibit discontinuity in hourly duration, which is also consistent with the update frequency of the broadcast ephemeris.

The error sequences of broadcast clock offset and the PPP-B2b clock offset referenced to GFZ precise clock offsets are presented in Figure 7a,b, respectively. As shown in Figure 7b, the continuity of the broadcast satellite clock offset is significantly improved by applying the PPP-B2b clock offset corrections. However, individual clock offset biases still exist in the clock offset error sequence. To effectively evaluate the accuracy of the PPP-B2b satellite clock offsets, the individual clock offset biases need to be corrected by subtracting the average clock offset, as described in re-edit Equations (9) and (10).

The series of re-edit clock offset differences of the broadcast satellite, and that of the PPP-B2b corrections, as well as the errors of WHU real-time clock offset are shown in Figure 8. The re-edit clock offset bias of the PPP-B2b becomes smoother and more continuous. As shown in Figure 8b, the clock offsets of PPP-B2b, however, clearly exhibit satellite-specified systematic errors. For example, the real-time PPP-B2b clock bias of satellite C35 reaches 5 ns, which results in more than 1.5 m systematic bias. The study revealed that these satellite-specified systematic errors are related to the pseudorange observations [28]. If carrier phase observations are used for positioning, the satellite-specified systematic errors can be absorbed by ambiguities [10,28].

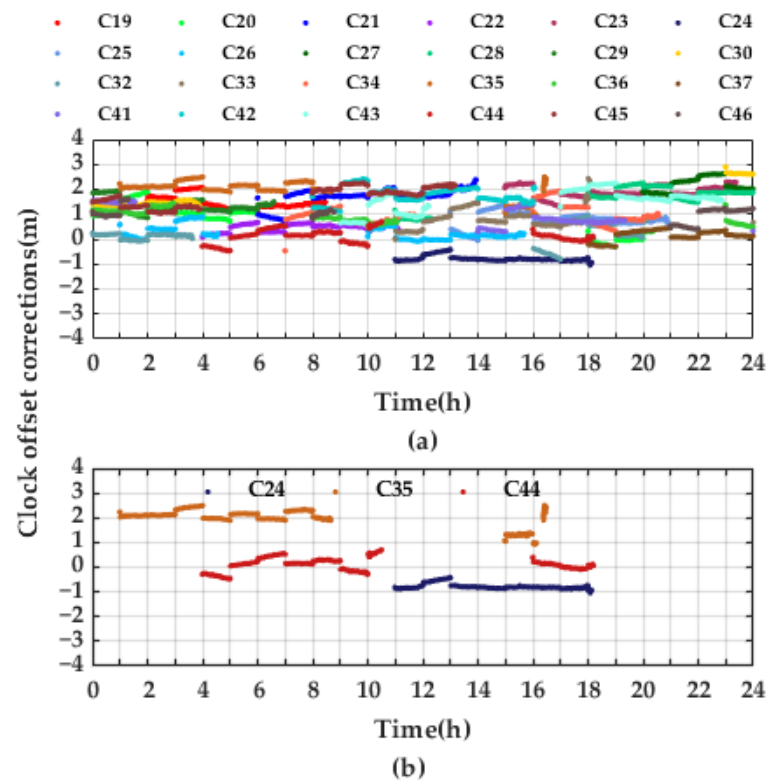


Figure 6. PPP-B2b clock offset corrections of all MEO satellites (a) and that of C24, C35, and C44 in detail (b).

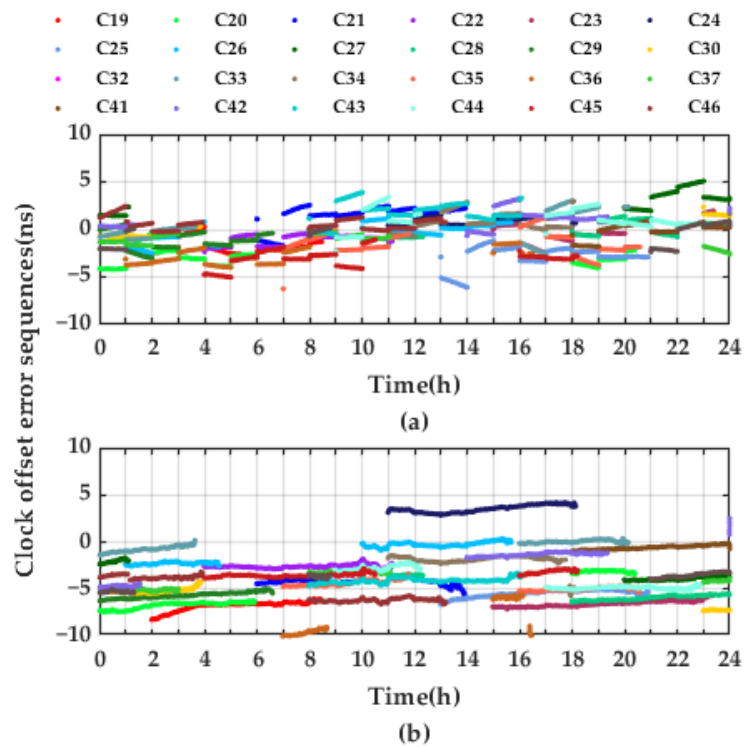
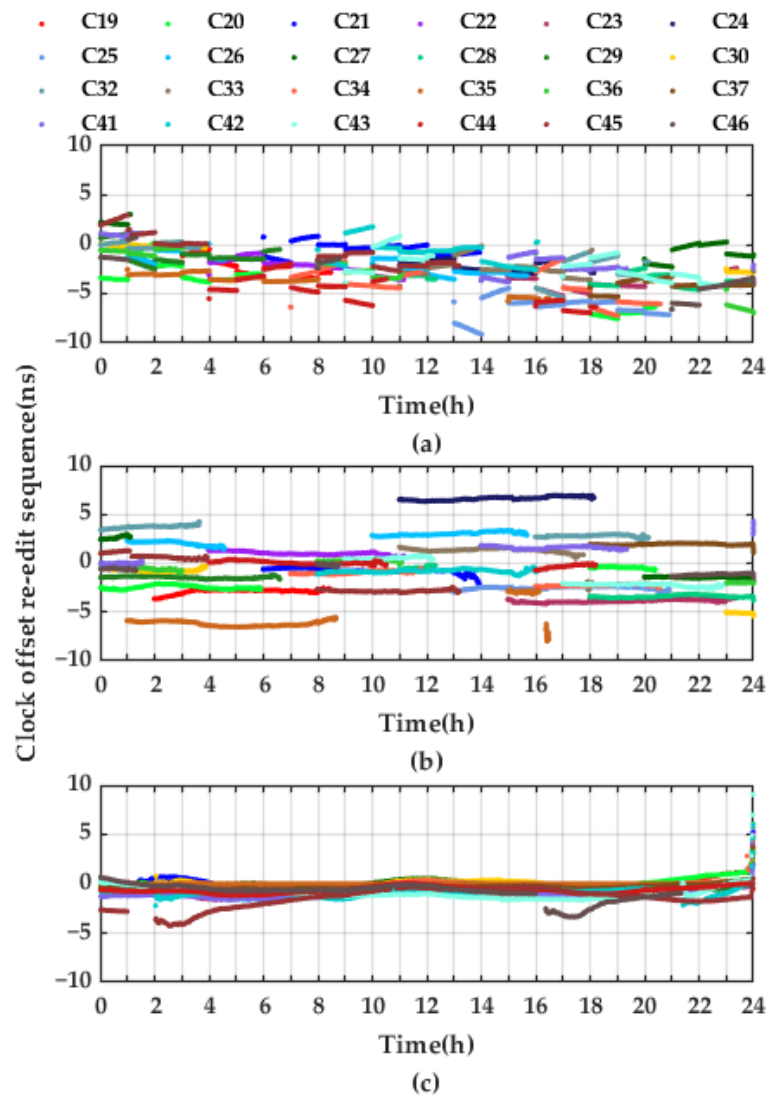
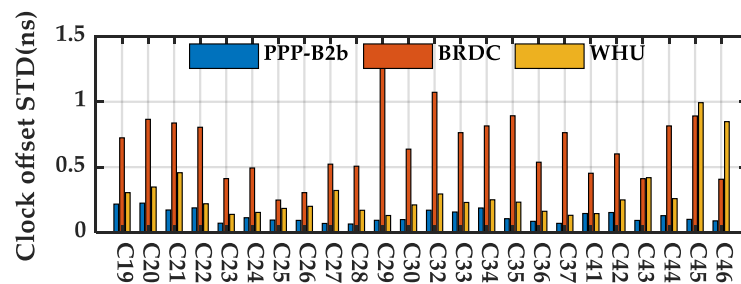


Figure 7. Satellite clock offset error sequences of broadcast clock offset (a) and PPP-B2b clock offset (b).



**Figure 8.** Satellite clock offset re-edit error sequences of broadcast clock offsets (a) and PPP-B2b clock offsets (b), WHU real-time clock offset (c).

As the satellite-specified systematic errors existed in the BDS-3 real-time clock products, the STD values acquired from re-edited error sequences of BDS-3 MEO satellites over a 7-day period are summarized and presented in Figure 9. The STD of PPP-B2b clock offsets is within 0.25 ns. The average STD of the PPP-B2b clock offsets is 0.124 ns, which is significantly improved compared to that of the broadcast clock offsets with the STD of 0.672 ns. The average STD of PPP-B2b clock offsets is also smaller than that of WHU real-time clock product, which is 0.360 ns.



**Figure 9.** Satellite clock offset STD.

### 3.3. PPP-B2b SISRE Performance Evaluation

The RMSs of SISRE and orbit only SISRE, as well as the STD of SISRE of broadcast ephemeris, PPP-B2b and WHU real-time products for BDS-3 MEO satellites during the 7d test period were calculated. The RMS SISRE of each satellite is plotted in Figure 10. The average RMS SISRE of broadcast ephemeris, PPP-B2b corrected products, and the real-time products from WHU are 0.536, 1.242, and 0.137 m, respectively. The largest SISRE of PPP-B2b occurred in satellite C35 with a value of 2.93 m, due to its outlying real-time clock offset with a value of 5 ns. The orbit only SISRE is plotted in Figure 11. The results show that the orbit only SISRE of PPP-B2b is similar to that of WHU real-time product. The abnormal SISRE value of PPP-B2b and the broadcast ephemeris on C41 and C42 are caused by PCO corrections. Thus, it can be confirmed that the large RMS SISRE value of PPP-B2b corrected products is mainly caused by the satellite-specified systematic error on clock offset. To exclude the systematic error effect on SISRE evaluation, the STD SISRE is also calculated and presented in Figure 12. The average STD SISRE of PPP-B2b is 0.097 m, which is similar to that of WHU real-time product. The average SISRE values are summarized in Table 3.

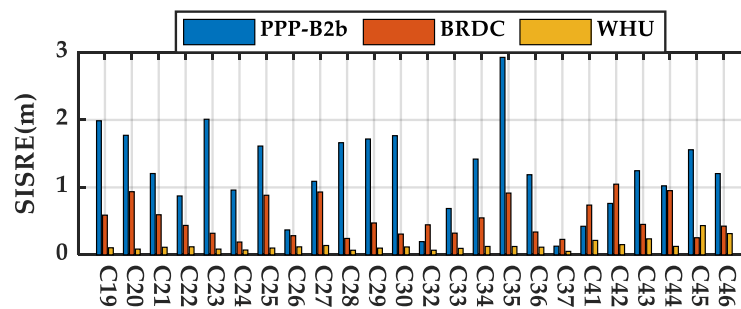


Figure 10. SISRE RMS of PPP-B2b, broadcast ephemeris, and WHU real-time products.

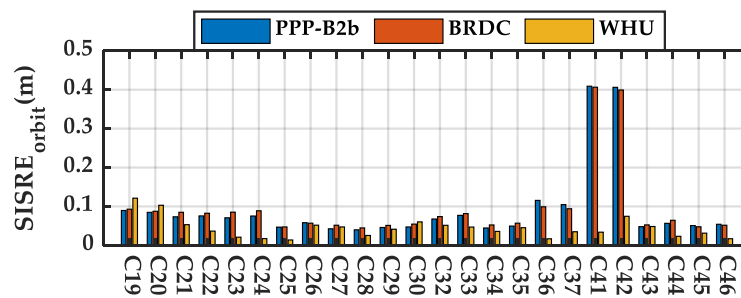


Figure 11. Orbit only SISRE RMS of PPP-B2b, broadcast ephemeris, and WHU real-time products.

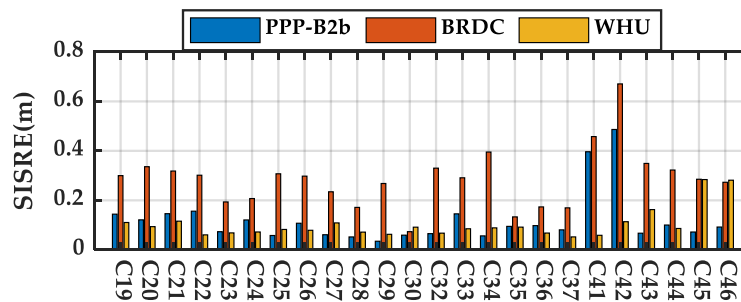


Figure 12. SISRE STD of PPP-B2b, broadcast ephemeris, and WHU real-time products.

**Table 3.** Average RMS and STD values of the SISRE for PPP-B2b, broadcast ephemeris, and WHU real-time products.

	PPP-B2b	Broadcast	WHU
SISRE RMS (m)	1.242	0.536	0.137
SISRE STD (m)	0.097	0.261	0.102

### 3.4. PPP-B2b DCB Accuracy Assessment

The PPP-B2b DCB and TGD from the broadcast ephemeris are converted to the same reference as the CAS DCB products. The PPP-B2b DCB, broadcast TGD, and CAS DCB of three signals, B1I, B1Cp, and B2ap, are plotted in Figure 13a,b,c, respectively. Differences between PPP-B2b DCB and CAS DCB, broadcast TGD and CAS DCB, are also plotted with blue and red bars in the corresponding figures. As shown in Figure 13a, the PPP-B2b DCBs and TGD of the B1I signal are consistent with that of CAS DCB. Some systematic errors exist between CAS DCB and PPP-B2b DCBs, as well as CAS DCB and the broadcast TGD of B1Cp and B2ap signals, as shown in Figure 13b,c, respectively. The biases on B1Cp and B2ap signals are 2 and 10 ns, respectively. In addition, the STD values of the B1I signal, B1Cp signal, and the B2ap signal are 0.46, 0.54, and 0.47 ns, respectively.

### 3.5. Real-Time PPP Positioning Accuracy Assessment

The positioning results on DOY 221 of eight IGS MEGX stations in China and surrounding counties were used to assess the positioning accuracy of the PPP-B2b services, as shown in Figure 14. The red dash indicates the service area of the PPP-B2b signal. The corresponding observation files were downloaded from the File Transfer Protocol Server (FTP) of GFZ. Both static and kinematic mode PPP were processed with B1I/B3I IF combinations. The processing strategies are shown in Table 4 in detail. In this section, three stations, JFNG, MIZU, and SGOC are employed, to demonstrate the performance of the PPP-B2b service. The JFNG station is located in China, while the MIZU station and the SGOC station are situated in Japan and Sri Lanka, the boundary of the PPP-B2b service area, as shown in Figure 14. The Position Dilution of Precision (PDOP) value, positioning accuracy, and convergence time of the three stations are analyzed in detail.

The visible satellites and available satellites with PPP-B2b corrections on DoY 221 are presented in Figure 15. During the selected test period, at least nine satellites of BDS-3 are visible at these three stations. The number of satellites with available PPP-B2b corrections, however, is less than that of visible satellites. As shown in Figure 15, the number of minimum available satellites is 4 at the SGOC station during the selected test period. The PPP-B2b service availability is further analyzed in these three stations. As shown in Figure 16, the visible satellites and visible periods are marked as red lines, while the available satellites with PPP-B2b correction and the available duration are marked with purple lines. It is clearly illustrated that the visible satellites of each station are similar, but the number of PPP-B2b available satellites of each station is different. In JFNG station, the number of available satellites is similar to that of visible satellites, and the PPP-B2b availability rate is 84.3%, while the availability rates of MIZU and SGOC stations are 74.6% and 57.2%, respectively. The availability rates of the three stations decrease as the stations are closer to the boundary of the service area.

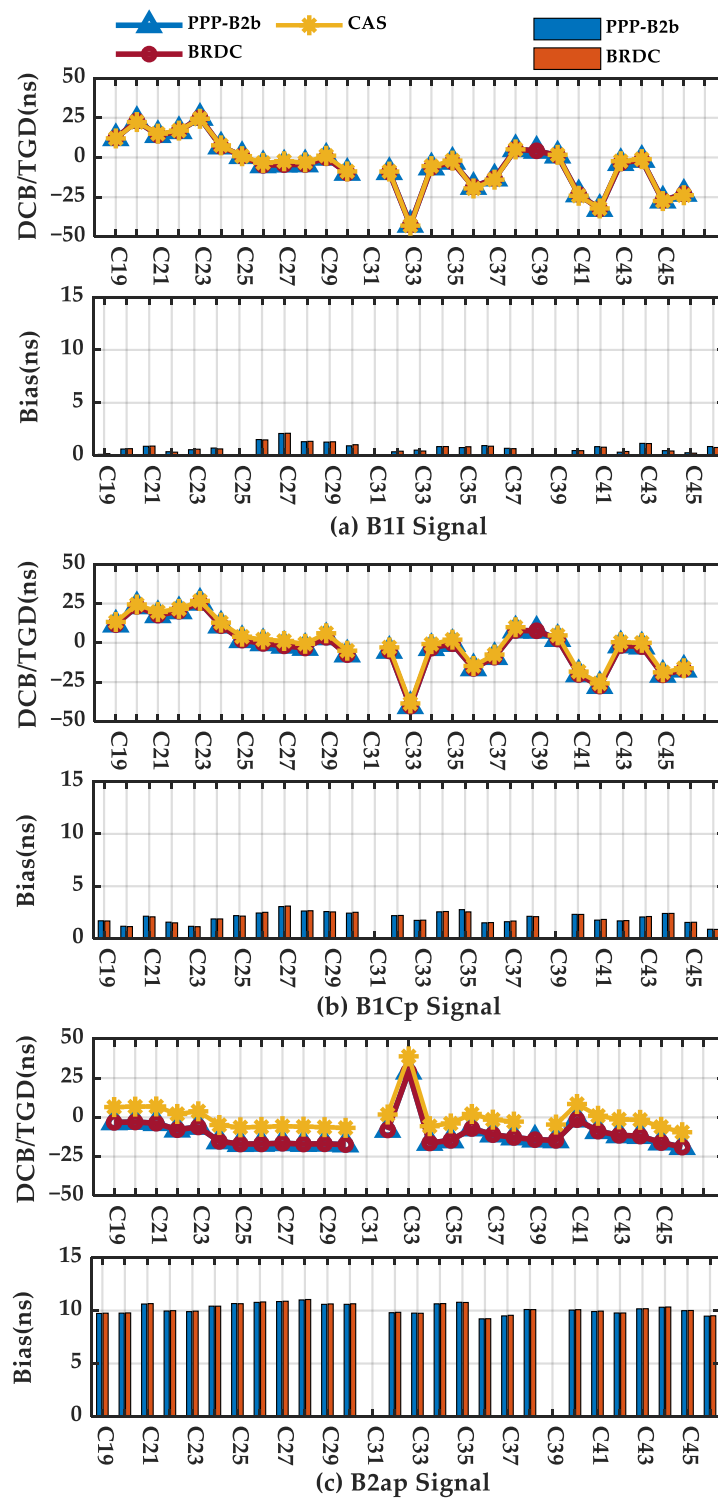


Figure 13. DCB or TGD corrections and corresponding bias of B1I signal (a), B1Cp signal (b), and B2ap signal (c).

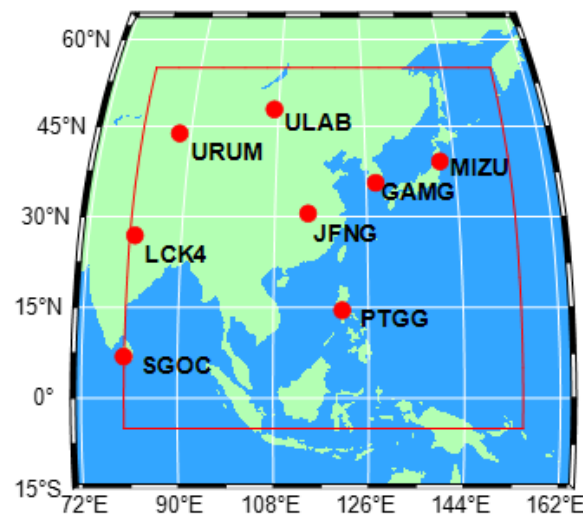


Figure 14. The map of selected stations.

Table 4. Real-time PPP processing strategy.

Item	Strategy/Model
Constellation	BDS-3
Sampling rate	30 s
Mode	Static/Kinematic
IF combination	B1I + B3I
Orbit/Clock offset	CNAV1 + PPP-B2b
DCB	PPP-B2b
Cutoff elevation	7°
Relativistic effect	Model corrected
Phase windup	Model corrected
Ionosphere	Eliminated by IF combination
Troposphere	Saastamoinen model corrects the zenith dry delay + Estimate zenith wet delay
Ambiguity	Estimated as a float constant

The PDOP is an important factor affecting the PPP positioning accuracy and convergence time [17,40,41]. The Dilution of Precision (DOP) matrix can be expressed as:

$$G = (H^T H)^{-1} \quad (17)$$

where  $H$  is the design matrix of PPP solutions as expressed in Equation (16). The PDOP is expressed as:

$$PDOP = \sqrt{G_{11} + G_{22} + G_{33}} \quad (18)$$

where  $G_{11}$ ,  $G_{22}$ , and  $G_{33}$  are the first three diagonal elements of the DOP matrix  $G$ . In our case, the PDOP is calculated according to the PPP-B2b available satellites.

The PDOP values of the JFNG, MIZU, and SGOC stations on DoY 221 are illustrated in Figure 17. The PDOP values of the JFNG station fluctuate around 2 with a maximum value of 6. The PDOP values of MIZU and SGOC stations fluctuate more widely compared with those of the JFNG station. The maximum PDOP value of the MIZU station is 42 at epoch 7 h:12 m:00 s, while that of the SGOC station is 67 at epoch 10 h:18 m:00 s. To further analyze the fluctuation in PDOP values of these three stations, the sky images at 10 h:18 m:00 s are drawn in Figure 18. At that epoch, the SGOC station has 11 visible satellites, including 5 satellites with PPP-B2b correction information, 4 of which are located on the north side of the SGOC station. Thus, the poor observation geometry results in the large value of PDOP.

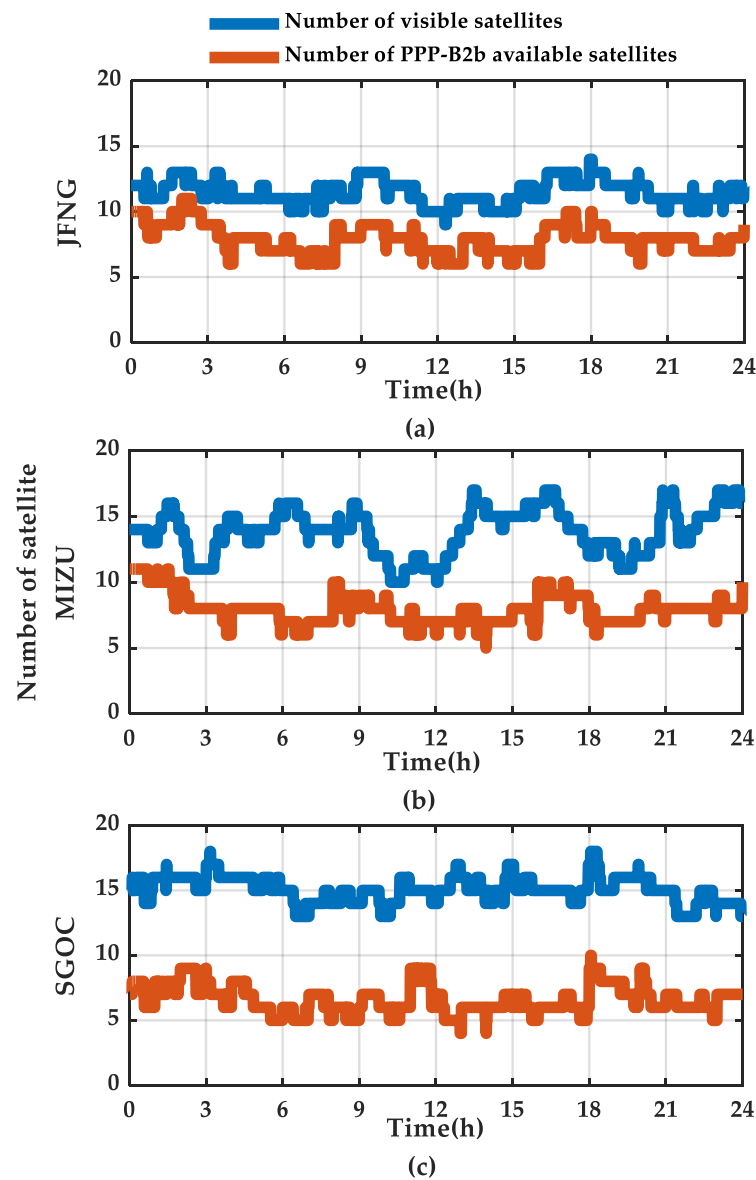


**Figure 15.** Number of visible satellites and number of PPP-B2b available satellites of (a) JFNG, (b) MIZU, and (c) SGOC.

The average number of visible satellites, the average number of PPP-B2b available satellites, and the corresponding availability rate, as well as the average PDOP values over 7 days for eight stations are listed in Table 5. The average PPP-B2b correction availability decreases as distance from the center of the PPP-B2b service area. The maximum PPP-B2b correction availability rate is 88.76% at the JFNG station, and the minimum availability rate of that is 60.91% at the SGOC station. The variation in average PDOP values showed similar trends, ranging from 2.55 to 4.47.

To illustrate the positioning performance of the PPP-B2b service, the PPP with WHU real-time products (WHU PPP) is also carried out to compare with the PPP-B2b results (B2b PPP). The positioning errors of B2b PPP and WHU PPP on the east (E), north (N), and up (U) components for the static positioning mode compared to the reference positions are presented in Figures 19 and 20, while the positioning errors in the kinematic positioning mode are presented in Figures 21 and 22, respectively.

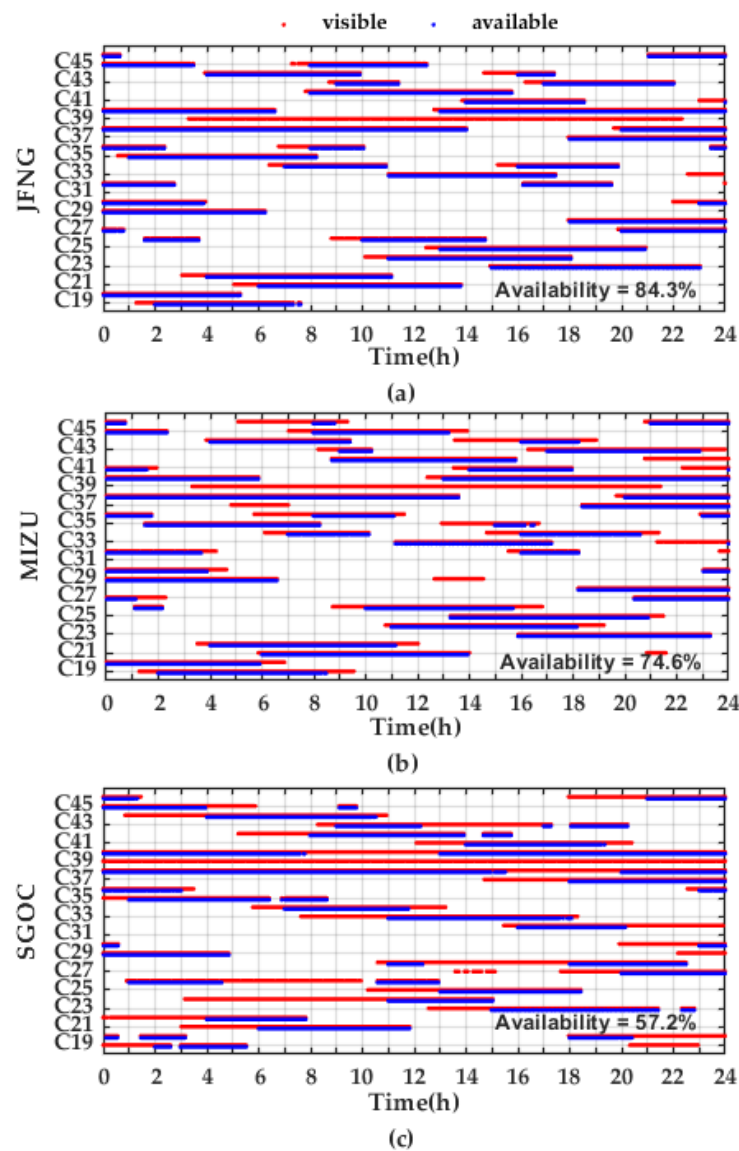


**Figure 16.** The visible satellites, the PPP-B2b available satellites, and the corresponding availability on DoY 221 of JFNG (a), MIZU (b), and SGOC (c).

In Figures 19 and 20, both B2b PPP and WHU PPP of the three stations achieve centimeter-level positioning accuracies after convergence. For B2b PPP, the positioning performance of the JFNG station, in terms of converge time and positioning accuracy, is better than that of the MIZU and the SGOC stations. For WHU PPP, the three stations present similar error levels, but the SGOC station needs longer convergence time on U components. The RMSE of E, N, and U components, as well as horizontal (H), and the three-dimensions (3D) for the eight stations on the static positioning mode based on the B2b PPP and WHU PPP are calculated and listed in Table 6. For B2b PPP, the RMSE on the E, N, and U components of all stations are similar, achieving centimeter-level accuracy. The RMSE of the N component is smaller than that of the E and U components in all stations. The RMSE of JFNG station on the E, N, and U components is slightly better than those of other stations due to the station being within the service area. The 3D errors vary between 3.9 and 8.3 cm. The performance of WHU PPP presents a similar trend as B2b PPP in the analyzed area. The RMSE of 3D error of each station based on the WHU PPP, however, is larger than that of B2b PPP in all stations. For example, for the JFNG station, the RMSE of 3D error is 3.9 cm for B2b PPP, while that of WHU PPP is 7.2 cm.

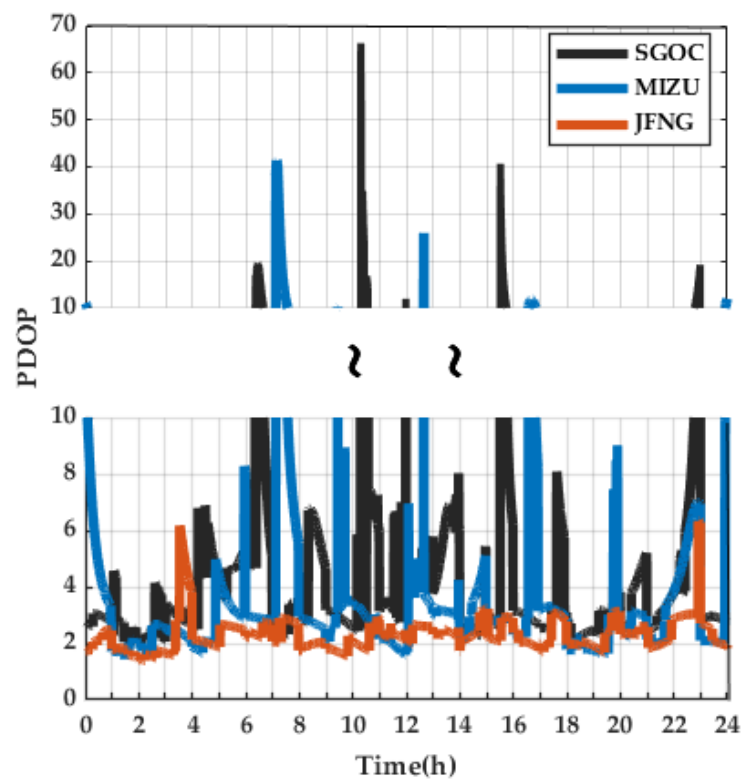


Figure 17. PDOP values on DoY 221 of three stations, JFNG, MIZU, and SGOC.

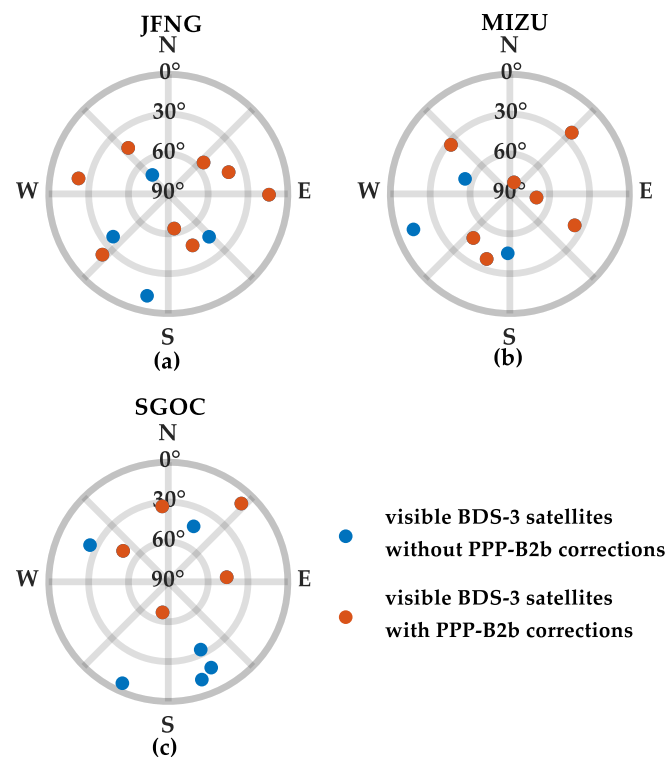
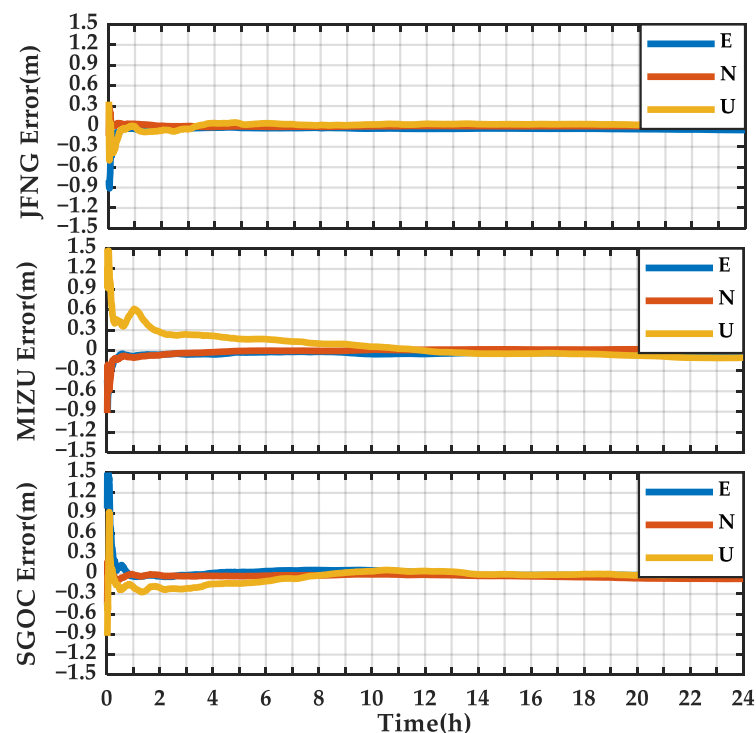


Figure 18. Sky images of JFNG (a), MIZU (b), and SGOC (c).

**Table 5.** Average number of visible satellites, average number of available satellites, average PPP-B2b correction availability rate, and average PDOP for each station.

Stations	Average Number of Visible Satellites	Average Number of Available Satellites	Average PPP-B2b Correction Availability Rate	Average PDOP
JFNG	11.41	8.29	88.76%	2.55
GAMG	13.92	8.92	83.22%	2.57
MIZU	13.71	8.37	78.97%	3.07
PTGG	13.96	7.83	73.03%	2.88
ULAB	14.14	8.15	81.19%	3.90
URUM	14.76	8.00	75.47%	4.24
LCK4	12.15	7.45	72.89%	3.94
SGOC	14.91	7.06	60.91%	4.47

**Figure 19.** Positioning error series of static positioning mode PPP (B2b PPP) on DoY 221.

In Figure 21, the positioning errors of B2b PPP at the JFNG on E, N, and U components are within 0.3 m after convergence for the kinematic positioning mode. The horizontal components of the positions of the MIZU and the SGOC stations are similar to those of the JFNG. The U component error of the MIZU and the SGOC stations, however, is relatively large compared to that of the JFNG station. The maximum error of the U component is at SGOC station with 1.3 m, which is caused by poor observation geometries and a lower number of available satellites with PPP-B2b corrections. The peak value can be easily observed on the SGOC station at epoch 10 h:18 m:00 s, 12 h:00 m:00 s, and 15 h:30 m:00 s, when the positioning error is larger than 0.9 m. The number of PPP-B2b available satellites at these epochs are less than 5, and the PDOP value is larger than 10, as shown in Figures 15 and 17. In Figure 22, the positioning errors of WHU PPP of the three stations are similar and all of them achieve decimeter-level accuracy. The positioning performance of the SGOC station with WHU PPP, compared to that of B2b PPP, is not affected by the number of PPP-B2b available satellites. The convergence time of WHU PPP, however, is slightly longer than that of B2b PPP.

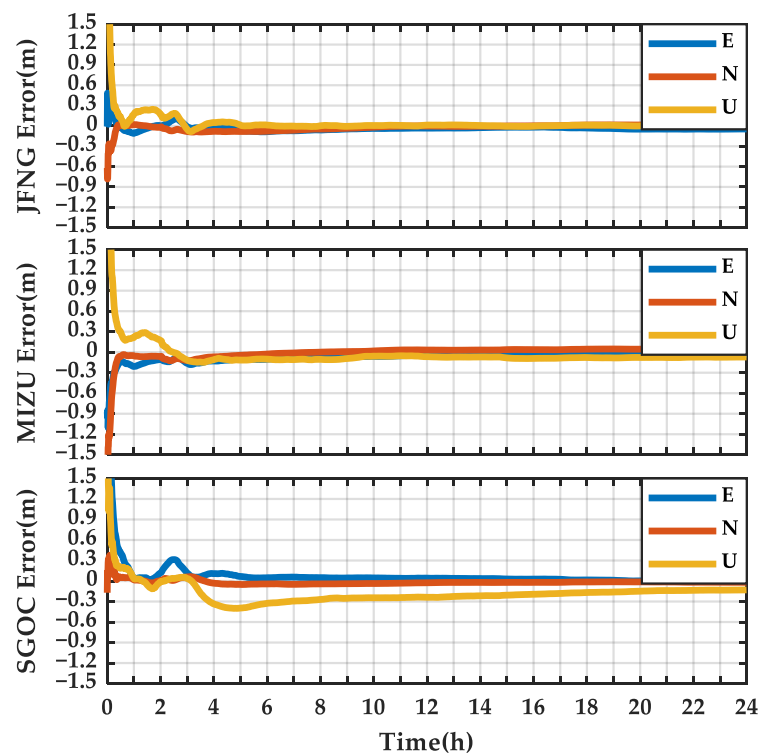


Figure 20. Positioning error series of static positioning mode PPP (WHU PPP) on DoY 221.

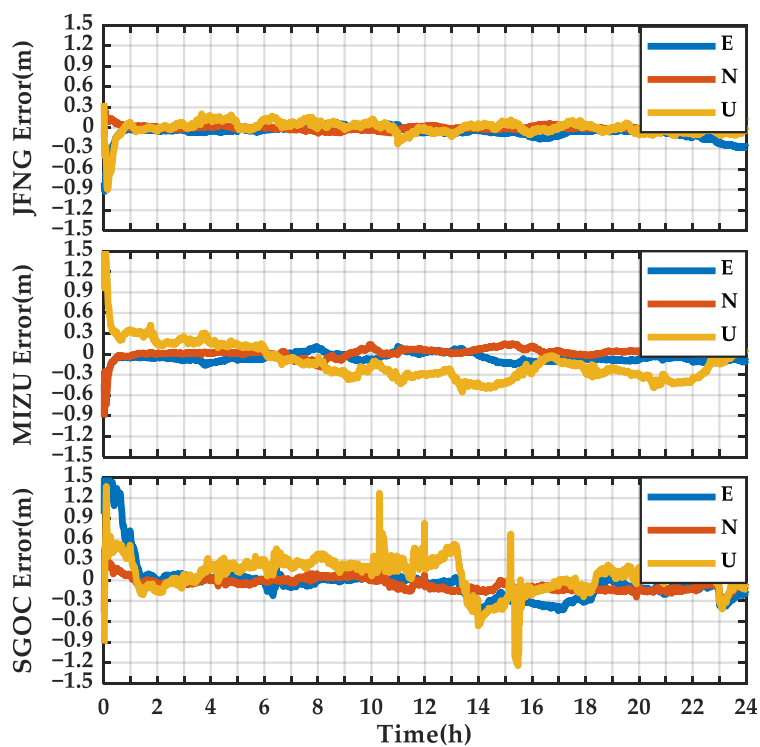


Figure 21. Kinematic mode PPP (B2b PPP) positioning error series of DoY 221.

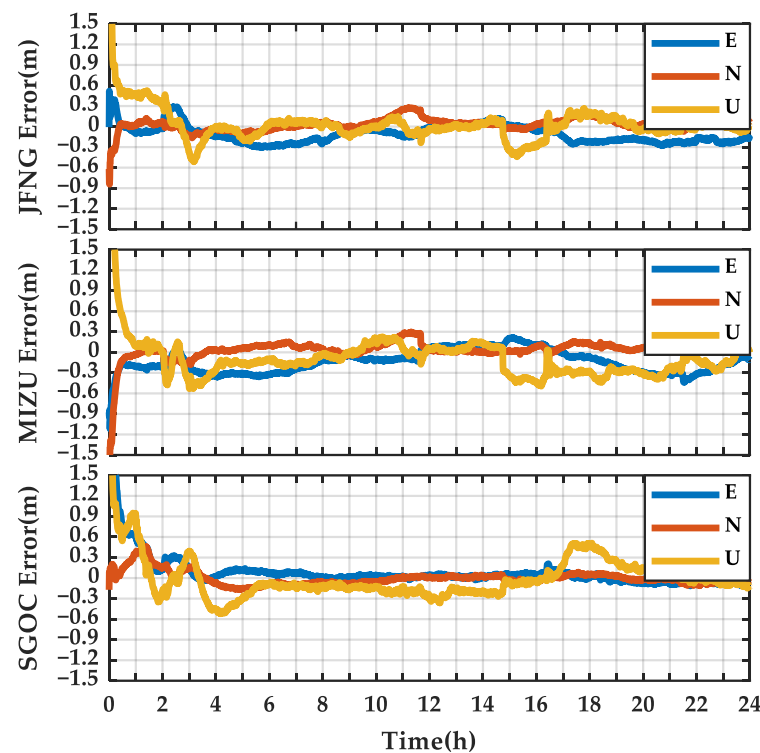


Figure 22. Kinematic mode PPP (WHU PPP) positioning error series of WHU on DoY 221.

Table 6. RMSE (cm) for each station on static positioning mode (B2b PPP vs. WHU PPP).

Stations	Static B2b PPP					Static WHU PPP				
	E	N	U	H	3D	E	N	U	H	3D
JFNG	3.3	0.5	2.1	3.4	3.9	5.2	3.5	3.6	6.3	7.2
GAMG	4.6	0.8	4.7	4.6	6.6	5.4	4.5	7.5	7.0	10.3
MIZU	3.6	1.2	4.9	3.8	6.2	5.9	4.6	11.8	7.5	14.0
PTGG	4.6	1.2	5.8	4.7	7.5	5.0	2.4	15.3	5.5	16.3
ULAB	5.9	0.7	3.6	5.9	6.9	4.9	4.0	7.9	6.3	10.1
URUM	3.6	2.3	7.1	4.3	8.3	3.0	2.3	7.5	3.8	8.4
LCK4	5.3	2.2	5.1	5.7	7.7	3.3	3.4	14.1	4.7	14.8
SGOC	3.5	2.2	3.3	4.1	5.3	4.9	2.8	10.8	5.6	12.2
mean	4.3	1.4	4.6	4.6	6.5	4.7	3.4	9.8	5.8	11.7

The RMSE of E, N, and U components, horizontal (H), and 3-dimensions (3D) for eight stations on kinematic positioning mode regarding B2b PPP and WHU PPP are calculated and listed in Table 7. The RMSE of the E, N, and U components of all stations achieve decimeter-level accuracy. The RMSE of the N component is smaller than that of the E and U components in all stations. For B2b PPP, the RMSE of the JFNG station on E, N, and U components are 7.3, 3.5, and 9.1 cm, respectively, while the errors of the three components at the SGOC station are 19.2, 9.2, and 21.3 cm, respectively, which are two times larger than that of JFNG station. Especially, for the RMSE of WHU PPP all eight stations present similar performance, achieving decimeter-level accuracy. For stations located on the service boundary, such as SGOC and LCK4, the RMSEs are smaller than those of B2b PPP. The RMSE values of different positioning strategies are summarized in Figure 23.

**Table 7.** RMSE (cm) for each station (B2b PPP vs. WHU PPP).

Stations	Kinematic B2b PPP					Kinematic WHU PPP				
	E	N	U	H	3D	E	N	U	H	3D
JFNG	7.3	3.5	9.1	8.1	12.2	12.9	7.9	16.5	15.1	22.4
GAMG	6.7	5.0	16.4	8.3	18.4	15.0	9.1	22.5	17.5	28.5
MIZU	6.8	5.9	14.7	9.0	17.2	12.9	10.1	28.3	16.4	32.7
PTGG	9.1	6.3	21.3	11.1	24.0	12.1	7.0	25.4	14.0	29.0
ULAB	7.8	6.0	15.1	9.8	18.0	16.1	9.8	24.8	18.8	31.1
URUM	15.4	5.1	11.6	16.2	19.9	15.5	8.1	28.1	17.5	33.1
LCK4	19.3	7.6	18.9	20.7	28.1	12.4	6.7	21.8	14.1	26.0
SGOC	19.2	9.2	21.3	21.3	30.1	13.6	9.2	15.9	16.4	22.9
Mean	11.5	6.1	16.1	13.1	21.0	13.8	8.5	22.9	16.2	28.2

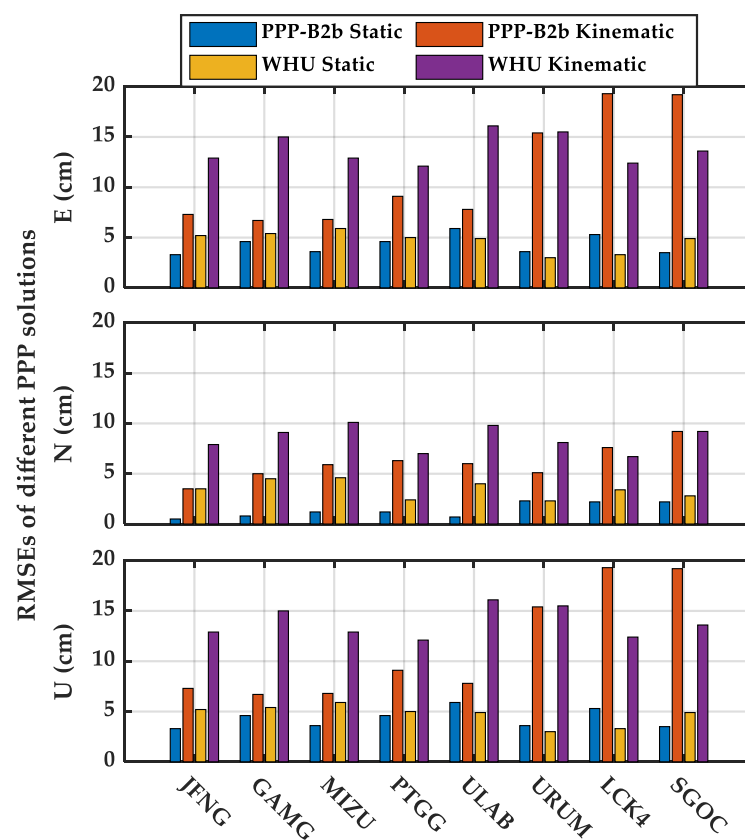


**Figure 23.** The RMSE summary of different positioning strategies.

To further evaluate the real-time performance of PPP-B2b services, the PPP with broadcast ephemeris is also carried out which is listed in Table 8. For the static positioning mode, the RMSE of horizontal components are similar, with decimeter-level accuracy. For the kinematic positioning mode, the RMSE of horizontal component is around 1.5 m.

The convergence time of these stations is also used to analyze the positioning performance. The convergence time for the static positioning mode is defined as the positioning error less than 10 cm on the E and N components and less than 30 cm on the U component, and lasts for at least 10 min. For the kinematic positioning mode, the convergence time is defined as the error within 30 cm on the E and N components, within 60 cm on the U component, and lasts for at least 10 min. The daily convergence time over 7 days of the eight stations is summarized in Table 9 with both B2b PPP and WHU PPP. In static positioning mode, for B2b PPP, the convergence time varies between 16.33 and 40.58 min except for the MIZU station. The convergence time of the MIZU station is 99.17 min due to the significant error on the U component at the beginning epochs, which is further caused

by the considerable value of PDOP, as shown in Figure 17. In kinematic positioning mode, B2b PPP, the convergence time varies between 11.08 and 45.66 min. The convergence time with B2b PPP is shorter than that of WHU PPP, which is mainly caused by the smaller STD on PPP-B2b clock offset.

**Table 8.** RMSE (m) of broadcast PPP.

Stations	Static					Kinematic				
	E	N	U	H	3D	E	N	U	H	3D
JFNG	0.22	0.61	1.22	0.65	1.38	0.94	1.39	3.08	1.68	3.51
GAMG	0.23	0.57	0.85	0.61	1.05	0.75	1.50	1.99	1.68	2.59
MIZU	0.41	0.67	0.92	0.79	1.21	0.73	1.32	1.93	1.51	2.45
PTGG	0.42	0.51	1.02	0.67	1.22	1.37	1.07	3.39	1.74	3.81
ULAB	0.23	0.62	1.35	0.67	1.50	0.94	1.52	2.96	1.79	3.46
URUM	0.29	0.17	1.25	0.34	1.29	1.23	1.11	2.29	1.66	2.83
LCK4	0.75	0.20	0.76	0.78	1.09	1.39	1.13	2.23	1.79	2.86
SGOC	0.49	0.21	0.50	0.53	0.73	1.28	1.00	2.06	1.62	2.62
Mean	0.38	0.45	0.98	0.63	1.18	1.08	1.26	2.49	1.68	3.01

**Table 9.** Convergence time (min) for each station.

Stations	B2b PPP		WHU PPP	
	Static	Kinematic	Static	Kinematic
JFNG	16.33	11.08	22.17	29.87
GAMG	23.83	14.75	27.84	30.36
MIZU	99.17	13.75	39.33	23.68
PTGG	17.91	27.75	46.00	14.83
ULAB	18.91	24.66	28.67	67.00
URUM	21.75	39.41	41.33	109.50
LCK4	29.58	32.75	45.85	99.14
SGOC	40.58	45.66	54.50	54.29

From the results of the experiments, we found that the positioning accuracy of the selected stations with real-time PPP-B2b service can achieve centimeter-level accuracy in static positioning mode and decimeter-level accuracy in kinematic positioning mode. The overall positioning performance of PPP-B2b service within the test area is slightly better than that of WHU real-time products. The reason may be that the service areas of the PPP-B2b are consistent with those of its monitoring network, while the WHU real-time products are calculated based on the global GNSS network which is not consistent with the test area. The positioning performance of stations located at the boundary of the service area, however, is worse than that of the WHU real-time product. The PPP with broadcast ephemeris can achieve decimeter level accuracy in static positioning mode in the selected stations, which also corresponds to the smaller value of SISRE of broadcast ephemeris, which is 0.536 m.

#### 4. Conclusions

The PPP-B2b signals transmitted by the GEO satellites of BDS-3 provide a real-time PPP service in China and the surrounding areas. In this study, we evaluated the performance of the PPP-B2b service within China and surrounding countries. The BDS-3 PPP-B2b performance in terms of satellite orbit and clock, SISRE, and DCB were evaluated related to those from GFZ final precise products and compared to those from the WHU real-time product. The PPP performance of PPP-B2b service was evaluated with comparison to PPP with WHU real-time products in both static and kinematic positioning modes. The following conclusions could be drawn:

1. The accuracy of the BDS-3 broadcast orbit is similar to that of the PPP-B2b real-time orbit. The RMSE of broadcast orbit is 8.8, 20.7, and 15.4 cm in radial, along-track, and cross-track components, respectively, while those of PPP-B2b orbits are 8.5, 19.3, and 14.0 cm, respectively. It should be emphasized that the difference between the broadcast orbit and PPP-B2b orbit is only centimeter-level due to the support of the inter-satellite links among the BDS-3 satellites. The PCO corrections from CSNO and IGS are different, which results in abnormal orbit bias in different satellites with different PCO corrections.
2. The satellite clock offset precision of the BDS-3 broadcast ephemeris is significantly improved by PPP-b2b clock corrections and improved the continuity of the broadcast clock offsets accordingly. The satellite-specified systematic errors exist in the PPP-B2b clock offsets, which further affects the SISRE of PPP-B2b. The STD of the real-time precise PPP-B2b clock offsets is within 0.2 ns, while the average STD of the broadcast satellite clock offsets is 0.672 ns.
3. The RMS SISRE of broadcast ephemeris is 0.536 m, and that of PPP-B2b is 1.24 m. Comparing the orbit only SISRE, we found that the large SISRE values of broadcast ephemeris and PPP-B2b are mainly caused by the satellite-specified systematic error of the clock offset. The STD of PPP-B2b SISRE is only 0.097 m, which is similar to that of WHU real-time products.
4. The DCB corrections in the message of PPP-B2b and broadcast TGD are compared with the CAS final DCB products. The STD values of DCB corrections relative to CAS DCB corrections are 0.46, 0.54, and 0.47 ns for B1I, B1Cp, and B2ap signals, respectively. The DCB corrections and broadcast TGD on B1Cp and B2ap signals with respect to those of CAS DCB, however, exhibit constant bias of about 2 and 10 ns.
5. The average availability rate of PPP-B2b service during the test period at the eight IGS stations is above 60%. The positioning accuracy of static positioning mode achieves centimeter-level accuracy with the PPP-B2b service, which is similar with the PPP solution by using WHU real-time products. For kinematic positioning mode, decimeter-level accuracy is achieved with the PPP-B2b service. The station JFNG located in China has the best positioning accuracy among the eight stations, with 7.3, 3.5, and 9.1 cm in the E, N, and U components, respectively, which is better than those of the PPP solutions with WHU real-time products. The RMSE of the positioning solution with the PPP-B2b service at the SGOC station, which is located at the boundary of the service area with considerable PDOP value, is two times larger than that of the JFNG station. The PPP solution on the SGOC station with WHU real-time product, however, has better positioning accuracy than that of the PPP-B2b service, which is not affected by the number of PPP-B2b available satellites. From our study, the PPP-B2b service has better positioning performance than that of WHU real-time products within the service coverage area in both static positioning mode and kinematic positioning mode.

**Author Contributions:** Conceptualization, C.Y.; Data curation, M.Z.; Funding acquisition, C.Y.; Investigation, Y.L. and C.Y.; Software, Y.L.; Supervision, C.Y.; Visualization, Y.L. and M.Z.; Writing—original draft, Y.L.; Writing—review & editing, C.Y. and Y.L. All authors have read and agreed to the published version of the manuscript.

**Funding:** This study is supported by the National Science Foundation of China (No. 41804036) and the National Key Research and Development Program of China (No. 2020YFB0505802).

**Institutional Review Board Statement:** Not applicable.

**Informed Consent Statement:** Not applicable.

**Data Availability Statement:** The datasets analyzed in this study are managed by the School of Land Science and Geomatics, China University of Geosciences, Beijing and can be available on request from the corresponding author.

**Acknowledgments:** The authors greatly appreciate IGMAS, GFZ, CAS, WHU, and CSNO for providing the necessary products.

**Conflicts of Interest:** The authors declare no conflict of interest.

## References

1. Yang, Y.X. Concepts of Comprehensive PNT and Related Key Technologies. *Acta Geod. Cartogr. Sin.* **2016**, *45*, 505–510.
2. Yang, Y.; Mao, Y.; Sun, B. Basic performance and future developments of BeiDou global navigation satellite system. *Satell. Navig.* **2020**, *1*, 1. [CrossRef]
3. Yang, Y.; Liu, L.; Li, J.; Yang, Y.; Zhang, T.; Mao, Y.; Sun, B.; Ren, X. Featured services and performance of BDS-3. *Sci. Bull.* **2021**, *66*, 2135–2143. [CrossRef]
4. Zumberge, J.F.; Heflin, M.B.; Jefferson, D.C.; Watkins, M.M.; Webb, F.H. Precise point positioning for the efficient and robust analysis of GPS data from large networks. *J. Geophys. Res.-Solid Earth* **1997**, *102*, 5005–5017. [CrossRef]
5. Jin, S.; Su, K. PPP models and performances from single- to quad-frequency BDS observations. *Satell. Navig.* **2020**, *1*, 16. [CrossRef]
6. Guo, J.; Geng, J.H.; Wang, C. Impact of the third frequency GNSS pseudorange and carrier phase observations on rapid PPP convergences. *GPS Solut.* **2021**, *25*, 30. [CrossRef]
7. Geng, J.; Guo, J.; Meng, X.; Gao, K. Speeding up PPP ambiguity resolution using triple-frequency GPS/BeiDou/Galileo/QZSS data. *J. Geod.* **2020**, *94*, 6. [CrossRef]
8. Li, P.; Jiang, X.; Zhang, X.; Ge, M.; Schuh, H. GPS + Galileo + BeiDou precise point positioning with triple-frequency ambiguity resolution. *GPS Solut.* **2020**, *24*, 78. [CrossRef]
9. Hong, J.; Tu, R.; Zhang, R.; Fan, L.; Zhang, P.; Han, J. Contribution analysis of QZSS to single-frequency PPP of GPS/BDS/GLONASS/Galileo. *Adv. Space Res.* **2020**, *65*, 1803–1817. [CrossRef]
10. Xu, Y.; Yang, Y.; Li, J. Performance evaluation of BDS-3 PPP-B2b precise point positioning service. *GPS Solut.* **2021**, *25*, 142. [CrossRef]
11. Dai, L.; Chen, Y.; Lie, A.; Zeitzew, M.; Zhang, Y. StarFire™ SF3: Worldwide Centimeter-Accurate Real Time GNSS Positioning. In Proceedings of the 29th International Technical Meeting of The Satellite Division of the Institute of Navigation (ION GNSS+ 2016), Portland, OR, USA, 12–16 September 2016; pp. 3295–3320.
12. Leandro, R.; Landau, H.; Nitschke, M.; Glocker, M.; Seeger, S.; Chen, X.; Deking, A.; BenTahar, M.; Zhang, F.; Ferguson, K.; et al. RTX Positioning: The Next Generation of cm-accurate Real-time GNSS Positioning. In Proceedings of the 24th International Technical Meeting of the Satellite Division of The Institute of Navigation (ION GNSS 2011), Portland, OR, USA, 20–23 September 2011; pp. 1460–1475.
13. Ge, Y.; Chen, S.; Wu, T.; Fan, C.; Qin, W.; Zhou, F.; Yang, X. An analysis of BDS-3 real-time PPP: Time transfer, positioning, and tropospheric delay retrieval. *Measurement* **2021**, *172*, 108871. [CrossRef]
14. Carlin, L.; Hauschild, A.; Montenbruck, O. Precise point positioning with GPS and Galileo broadcast ephemerides. *GPS Solut.* **2021**, *25*, 77. [CrossRef]
15. Lu, X.; Chen, L.; Shen, N.; Wang, L.; Jiao, Z.; Chen, R. Decoding PPP Corrections From BDS B2b Signals Using a Software-Defined Receiver: An Initial Performance Evaluation. *IEEE Sens. J.* **2021**, *21*, 7871–7883. [CrossRef]
16. Nie, Z.; Xu, X.; Wang, Z.; Du, J. Initial Assessment of BDS PPP-B2b Service: Precision of Orbit and Clock Corrections, and PPP Performance. *Remote Sens.* **2021**, *13*, 2050. [CrossRef]
17. Tao, J.; Liu, J.; Hu, Z.; Zhao, Q.; Chen, G.; Ju, B. Initial Assessment of the BDS-3 PPP-B2b RTS compared with the CNES RTS. *GPS Solut.* **2021**, *25*, 131. [CrossRef]
18. Ren, Z.; Gong, H.; Peng, J.; Tang, C.; Huang, X.; Sun, G. Performance assessment of real-time precise point positioning using BDS PPP-B2b service signal. *Adv. Space Res.* **2021**, *68*, 3242–3254. [CrossRef]
19. China Satellite Navigation Office. BeiDou Navigation Satellite System Signal in Space Interface Control Document: Precise Point Positioning Service Signal PPP-B2b (Version 1.0). Available online: <http://en.beidou.gov.cn/SYSTEMS/ICD/202008/P020200803538771492778.pdf> (accessed on 20 October 2021).
20. Montenbruck, O.; Teunissen, P. Springer Handbook of Global Navigation Satellite Systems. In *Springer Handbooks*; Online Resource XXXI, 1327 Pages 818 Illustrations in Color; Springer International Publishing: Cham, Switzerland, 2017; p. 1.
21. Sošnica, K.; Zajdel, R.; Bury, G.; Bosy, J.; Moore, M.; Masoumi, S. Quality assessment of experimental IGS multi-GNSS combined orbits. *GPS Solut.* **2020**, *24*, 54. [CrossRef]
22. Montenbruck, O.; Steigenberger, P.; Hauschild, A. Broadcast versus precise ephemerides: A multi-GNSS perspective. *GPS Solut.* **2014**, *19*, 321–333. [CrossRef]
23. Shi, Y.; Hao, J.; Liu, W.; Jiao, B.; Zhang, H.; Song, B. Performance Assessment of BDS Real-Time Precise Point Positioning Based on SSR Corrections. *J. Surv. Eng.* **2019**, *145*, 05019003. [CrossRef]
24. China Satellite Navigation Office. BeiDou Navigation Satellite System Signal in Space Interface Control Document: Open Service Signal B1C (Version 1.0). Available online: <http://www.beidou.gov.cn/xt/gfzx/201712/P020171226741342013031.pdf> (accessed on 30 December 2021).
25. Montenbruck, O.; Steigenberger, P.; Hauschild, A. Multi-GNSS signal-in-space range error assessment—Methodology and results. *Adv. Space Res.* **2018**, *61*, 3020–3038. [CrossRef]

26. Yao, Y.; He, Y.; Yi, W.; Song, W.; Cao, C.; Chen, M. Method for evaluating real-time GNSS satellite clock offset products. *GPS Solut.* **2017**, *21*, 1417–1425. [[CrossRef](#)]
27. Xue, B.; Wang, H.; Yuan, Y. Performance of BeiDou-3 signal-in-space ranging errors: Accuracy and distribution. *GPS Solut.* **2021**, *25*, 23. [[CrossRef](#)]
28. Lv, Y.; Geng, T.; Zhao, Q.; Xie, X.; Zhou, R. Initial assessment of BDS-3 preliminary system signal-in-space range error. *GPS Solut.* **2019**, *24*, 16. [[CrossRef](#)]
29. Zhang, W.; Lou, Y.; Song, W.; Sun, W.; Zou, X.; Gong, X. Initial assessment of BDS-3 precise point positioning service on GEO B2b signal. *Adv. Space Res.* **2022**, *69*, 690–700. [[CrossRef](#)]
30. Wu, W.; Guo, F.; Zheng, J. Analysis of Galileo signal-in-space range error and positioning performance during 2015–2018. *Satell. Navig.* **2020**, *1*, 6. [[CrossRef](#)]
31. Kazmierski, K.; Zajdel, R.; Sośnica, K. Evolution of orbit and clock quality for real-time multi-GNSS solutions. *GPS Solut.* **2020**, *24*, 111. [[CrossRef](#)]
32. Wang, N.; Yuan, Y.; Li, Z.; Montenbruck, O.; Tan, B. Determination of differential code biases with multi-GNSS observations. *J. Geod.* **2015**, *90*, 209–228. [[CrossRef](#)]
33. Dai, P.; Xing, J.; Ge, Y.; Yang, X.; Qin, W.; Dong, Y.; Zhang, Z. The Effect of BDS-3 Time Group Delay and Differential Code Bias Corrections on Positioning. *Appl. Sci.* **2020**, *11*, 104. [[CrossRef](#)]
34. Zhang, B.; Zhao, C.; Odolinski, R.; Liu, T. Functional model modification of precise point positioning considering the time-varying code biases of a receiver. *Satell. Navig.* **2021**, *2*, 11. [[CrossRef](#)]
35. An, X.; Meng, X.; Jiang, W. Multi-constellation GNSS precise point positioning with multi-frequency raw observations and dual-frequency observations of ionospheric-free linear combination. *Satell. Navig.* **2020**, *1*, 7. [[CrossRef](#)]
36. Wang, W.; Wang, Y.; Yu, C.; Xu, F.; Dou, X. Spaceborne atomic clock performance review of BDS-3 MEO satellites. *Measurement* **2021**, *175*, 109075. [[CrossRef](#)]
37. Sakic, P.; Mansur, G.; Mannel, B. A prototype for a Multi-GNSS orbit combination. In Proceedings of the 2020 European Navigation Conference (ENC), Dresden, Germany, 23–24 November 2020.
38. Yang, Y.; Xu, Y.; Li, J.; Yang, C. Progress and performance evaluation of BeiDou global navigation satellite system: Data analysis based on BDS-3 demonstration system. *Sci. China-Earth Sci.* **2018**, *61*, 614–624. [[CrossRef](#)]
39. China Satellite Navigation Office. BeiDou Navigation Satellite System Open Service Performance Standard (Version 3.0). 2021. Available online: <http://m.beidou.gov.cn/xt/gfzx/202105/P020210526216231136238.pdf> (accessed on 11 November 2021).
40. Biswas, S.K.; Qiao, L.; Dempster, A. Effect of PDOP on performance of Kalman Filters for GNSS-based space vehicle position estimation. *GPS Solut.* **2017**, *21*, 1379–1387. [[CrossRef](#)]
41. Teng, Y.; Wang, J. Some Remarks on PDOP and TDOP for Multi-GNSS Constellations. *J. Navig.* **2015**, *69*, 145–155. [[CrossRef](#)]